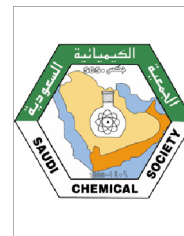




King Saud University  
Journal of Saudi Chemical Society

www.ksu.edu.sa  
www.sciencedirect.com



## ORIGINAL ARTICLE

# Preparation, characterization and catalytic properties of nickel aluminate nanoparticles: A comparison between conventional and microwave method

C. Ragupathi <sup>a</sup>, J. Judith Vijaya <sup>a,\*</sup>, L. John Kennedy <sup>b</sup>

<sup>a</sup> Catalysis and Nanomaterials Research Laboratory, Department of Chemistry, Loyola College, Chennai 34, India

<sup>b</sup> Materials Division, School of Advanced Sciences, Vellore Institute of Technology (VIT) University, Chennai Campus, Chennai 127, India

Received 14 August 2013; revised 9 January 2014; accepted 26 January 2014

## KEYWORDS

Nickel aluminate nanoparticle;  
Microwave method;  
Conventional method;  
Catalytic oxidation;  
*Opuntia dilenii haw*

**Abstract** In the present work, synthesis of nickel aluminate using *Opuntia dilenii haw* as plant extract by a microwave combustion method (MCM) and its comparison with the conventional combustion method (CCM) is investigated. *O. dilenii haw* plant extract simplifies the process, provides an alternative process for a simple and an economical synthesis. The absence of surfactant has led to a simple, cheap and fast method of synthesis of NiAl<sub>2</sub>O<sub>4</sub> nanoparticles. The as-synthesized NiAl<sub>2</sub>O<sub>4</sub> nanoparticles were characterized by X-ray diffraction (XRD) studies, Fourier transform infrared spectroscopy (FT-IR) studies, high resolution scanning electron microscopy (HR-SEM), energy dispersive X-ray analysis (EDX), high resolution transmission electron microscopy (HR-TEM), diffuse reflectance spectroscopy (DRS), and Brunauer Emmett Teller (BET) surface area analysis. The XRD results confirmed the formation of the cubic phase NiAl<sub>2</sub>O<sub>4</sub>. The formation of pure nickel aluminate phase was confirmed by FT-IR. The formation of NiAl<sub>2</sub>O<sub>4</sub> nanoparticles was confirmed by HR-SEM and HR-TEM and their possible formation mechanisms were also proposed. MCM could produce NiAl<sub>2</sub>O<sub>4</sub> with uniform size and well-defined shape with crystallinity. The optical property was determined by DRS. NiAl<sub>2</sub>O<sub>4</sub> prepared by the microwave combustion method was found to possess a higher surface area, lower crystallite size than the NiAl<sub>2</sub>O<sub>4</sub> nanoparticles prepared by the conventional combustion method, which in turn has led to the improved performance toward the selective oxidation of benzyl alcohol to benzaldehyde.

© 2014 King Saud University. Production and hosting by Elsevier B.V. All rights reserved.

\* Corresponding author. Tel.: +91 44 28178333; fax: +91 44 28175566.

E-mail addresses: [jjvijayaloyola@yahoo.co.in](mailto:jjvijayaloyola@yahoo.co.in), [jjvijaya78@gmail.com](mailto:jjvijaya78@gmail.com) (J.J. Vijaya).

Peer review under responsibility of King Saud University.



Production and hosting by Elsevier

## 1. Introduction

Nanostructured mixed metal oxides have attracted considerable attention in view of their potential applications in the areas, such as, ceramics, semiconductors, sensors, and catalytic materials [24,12,10,36]. Among the metal aluminates, NiAl<sub>2</sub>O<sub>4</sub> belongs to the spinel group, which has a general formula

1319-6103 © 2014 King Saud University. Production and hosting by Elsevier B.V. All rights reserved.

<http://dx.doi.org/10.1016/j.jscs.2014.01.006>

Please cite this article in press as: C. Ragupathi et al., Preparation, characterization and catalytic properties of nickel aluminate nanoparticles: A comparison between conventional and microwave method, Journal of Saudi Chemical Society (2014), <http://dx.doi.org/10.1016/j.jscs.2014.01.006>

$AB_2O_4$ , where  $A^{2+}$  and  $B^{3+}$  are divalent and trivalent cations, respectively and belongs to the space group  $Fd_3m$ . Nickel aluminates are among those that have widespread commercial value in the catalytic applications ranging from methane/steam and methanol reforming to hydrocarbon cracking, dehydrogenation, hydrodesulfurization, and hydrodenitrogenation [6,32,30]. Nickel aluminate spinel can be prepared by several methods, such as, solid-state reaction [35], sol-gel method [17], and wet chemical methods like hydrothermal and solvothermal method [39]. However, combustion synthesis is an easy and convenient method for the preparation of a variety of advanced ceramics, catalysts and nanomaterials. In this method, based on the principles of the propellant chemistry, a thermally induced redox reaction takes place between an oxidant and a fuel. By combustion-based methods, it is possible to produce the monophasic nano powders with homogeneous nano-microstructure at lower temperatures and/or shorter reaction times, when compared with the other methods [8].

Moreover, MCM offers great advantages such as, prompting the rapid reaction, due to the molecular level interaction of the microwave radiations with the reactant species. It is a clean, cheap, and convenient method of heating that often results in uniform particle morphology, shorter reaction time, and a promising method for the preparation for various nano-structured materials with different sizes and shapes. Moreover, it is environment-friendly, simple to operate, and energy efficient over the conventional combustion methods [14].

The fuel also forms complexes with the metal ions, facilitating the homogeneous mixing of the cations in the solution. Different types of fuels can also be used in the combustion synthesis. Currently, a restricted category of organic substances, organic polymers, such as, polyethylene glycol (PEG), polyvinyl alcohol (PVA), poly-acrylic acid (PAA), and a starch-derived polymer are used as the gelling or complexing agents. The sample decomposes burns and releases a large amount of heat and gases.

Recently, the photosynthesis method employs the plant extracts, which have emerged as a simple and viable alternative to the chemical synthetic procedures and physical methods. Nowadays, plant extracts have been used as both reducing and gelling agent for the synthesis of nanomaterials, which could be advantageous over photochemical reduction, heat evaporation, and other chemical reduction methods [2,38].  $ZnAl_2O_4$  nanoparticles were prepared by using sucrose as a chelating agent, which has been reported by A.G. Khaledi et al. Therefore, sucrose can also act as an effective gelling agent to produce fine particles of  $ZnAl_2O_4$  [18]. The plant extract used as a fuel has a coordinating action, capturing the involved metal ions in the amylose helix of the extract in well-defined sites, and impeding the separation of metal oxides.

*Opuntia dillenii haw* is found mainly in the southern parts of India. Further determination of the sugars showed that 8–10% hexoses and 0.98% pentoses are present. The major components of *O. dillenii haw* consist of a mixture of mucilage and pectin. Pectin is the most abundant polysaccharide present in *O. dillenii haw* [11]. And, it contains vitamin A, B1, B6, and E and also appreciable amounts of sucrose, maleic, malonic, succinic, tartaric and oxalic acid [15]. The synthesis using *O. dillenii haw* extract provides a simple, efficient and photosynthesis route for the synthesis of nanomaterials. The slow reductions along with the shape-directing effects of the constituents

of the plant extract play a key role in the formation of nano-structured metal oxides [33,4].

In the present work, we report for the first time, the synthesis of nano nickel aluminate by MCM, using the metal nitrates and *O. dillenii haw* plant extract solution as the precursors. Later, we compared the properties with the  $NiAl_2O_4$  nanoparticles prepared by CCM.  $NiAl_2O_4$  nanoparticles prepared by both CCM and MCM are tested for the catalytic activity toward the oxidation of benzyl alcohol.

## 2. Experimental section

### 2.1. Materials

Nickel nitrate and aluminum nitrate were used as the precursors (Merck chemicals, India) and were used without further purification.

### 2.2. Preparation of *O. dillenii haw* plant extract

The *O. dillenii haw* leaves were collected from the local agricultural fields at Pattaibiram, Chennai, Tamil Nadu, India. In the first process, about 10 g portion of thoroughly washed to properly remove the skin, it is most of the valuable inner gel of the leaf. In the second process, the inner gel portion was extracted from the *O. dillenii haw* leaves, which was finely cut and dissolved in 20 ml of de-ionized water, and stirred for 45 min to obtain a clear solution. The resulting extract was used as an *O. dillenii haw* plant extract solution.

### 2.3. Synthesis of $NiAl_2O_4$ by both CCM and MCM

Nickel nitrate and aluminum nitrate were dissolved in de-ionized water and then mixed with *O. dillenii haw* plant extract solution under constant stirring for 5 h, at room temperature until a clear transparent solution was obtained. The molar ratio of Ni/Al was kept as 1:2. The solution was dried in an air oven at 120 °C for 5 h. The resultant sample was then sintered at 600 °C at a heating rate of 5 °C/min for 3 h in muffle furnace, and it is labeled as sample A.

The clear transparent solution prepared as mentioned in the previous section was then placed in a domestic microwave oven (2.45 GHz, 950 W) for 20 min. Initially, the solution boiled and underwent dehydration followed by decomposition with the evolution of gases. It vaporized the solution, instantly became a solid, and it is labeled as sample B.

The fuel used is the plant extract, which exhibits both reducing and gelling agent. During the combustion, the gaseous products released were  $N_2$ ,  $NO_2$ ,  $CO_2$  and  $H_2O$  as water vapor. We assume that the fumes observed during combustion were released in the form of the above gaseous products.

### 2.4. Characterization of samples A and B

The structural studies were carried out using a Philips X' pert diffractometer for  $2\theta$  values ranging from 10° to 80° using Cu  $K\alpha$  radiation at  $\lambda = 0.154$  nm. A Perkin Elmer infrared spectrophotometer was used for the determination of the surface functional groups of the nanomaterials. Morphological studies and energy dispersive X-ray analysis of nanomaterial were per-

formed using a Joel JSM6360 high resolution scanning electron microscope Stereo-scan LEO 440 and a high resolution transmission electron microscope (HR-TEM). The diffuse reflectance UV–visible spectra of the nanomaterial were recorded using Cary100 UV–visible spectrophotometer. The nitrogen adsorption–desorption isotherms of the samples were measured using an automatic adsorption instrument (Quantachrome Quadrawin gas sorption analyzer) for the determination of surface area and total pore volumes. The diffuse reflectance UV–visible spectra of the nanomaterials were recorded using Cary100 UV–visible spectrophotometer.

### 2.5. Catalytic test

The oxidation of benzyl alcohol was carried out in a batch reactor operated under atmospheric conditions. 10 mmol of oxidant ( $\text{H}_2\text{O}_2$ ) was added with 0.5 g of the nano nickel aluminate (sample A and B) and the contents were heated at 80 °C in acetonitrile medium for 8 h in a three necked round bottom flask equipped with a reflux condenser and thermometer. The oxidized products after the catalytic reaction were collected and studied using Agilent GC spectrometer. The column used for the study was DB wax column (capillary column) of length 30 mm and helium was used as the carrier gas. GC technique was carried out to know the conversion percentage of the products formed.

## 3. Results and discussion

### 3.1. X-ray diffraction analysis

The XRD pattern of the prepared samples is given in Fig. 1(a and b). Fig. 1a showed the XRD pattern of the sample A (prepared by CCM), and Fig. 1b, displayed the XRD pattern of sample B (prepared by MCM) using *O. dillenii haw* plant extract that is used as both reducing and gelling agent. It revealed that both the samples A and B had the same crystalline structure. The diffraction peaks of the particles matched well with the diffraction data from the JCPDS card no. 10–0339. The peaks at  $2\theta$  values of 19.06, 31.40, 37.00, 44.99, 55.73, 59.65, and 65.53 correspond to the (1 1 1), (2 2 0), (3 1 1), (4 0 0), (4 2 2), (5 1 1), and (4 4 0) planes of  $\text{NiAl}_2\text{O}_4$  crystal, respectively, which can be readily assigned to a cubic phase  $\text{NiAl}_2\text{O}_4$  (space group  $\text{Fd}\bar{3}\text{m}$ ). No characteristic peak related to any other impurity was observed.

Further observation revealed that the samples A and B had the sharp peaks, which indicate the good crystallinity, but the diffraction peaks for the sample B were slightly broadened, due to the smaller crystallite size.

The average crystallite size for both the samples A and B was calculated using Scherrer formula [3].

$$L = \frac{0.89\lambda}{\beta \cos \theta}$$

where,  $L$ , average crystallite size, ( $\text{Å}$ ),  $\lambda$ , the X-ray wavelength (0.154 nm),  $\theta$ , the diffraction angle and  $\beta$ , the full-width at half maximum of the observed peaks. The average crystallite size for both the samples A and B was found to be 19.9 and 16.4 nm, respectively. Compared with the CCM method, MCM is more time-saving. But, both the obtained nickel aluminate nanoparticles have the same crystalline structure.

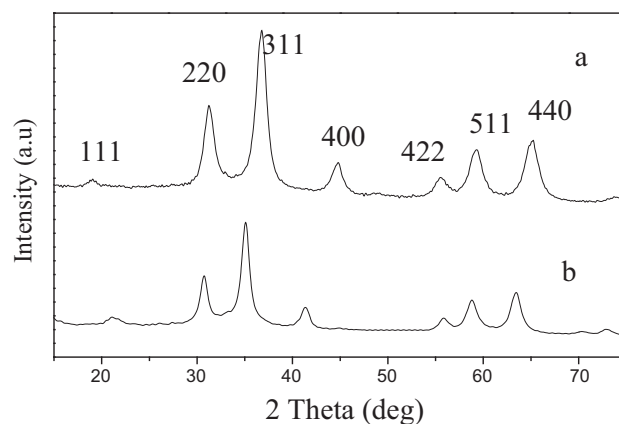


**Figure 1** XRD pattern of (a)  $\text{NiAl}_2\text{O}_4$ -sample A prepared by CCM (b)  $\text{NiAl}_2\text{O}_4$ -sample B prepared by MCM.

### 3.2. Fourier transform infrared (FT-IR) analysis

The FT-IR spectra Fig. 2(a and b) of  $\text{NiAl}_2\text{O}_4$  samples prepared by both CCM and MCM exhibited a broad band near  $3450\text{ cm}^{-1}$ , due to the  $-\text{OH}$  stretching vibration of free hydrogen bonded hydroxyl groups, and a second typical absorption band at  $1620\text{ cm}^{-1}$  is assigned to the deformative vibration of water molecules, which is most probably, due to the water absorption by the samples during the compaction of the powder  $\text{NiAl}_2\text{O}_4$  with KBr as pellets [37]. The absorption band of sample B (Fig. 2b) undergoes a red shift for water molecule from  $3476$  to  $3438\text{ cm}^{-1}$ , and from  $1636$  to  $1627\text{ cm}^{-1}$ , and then became weaker, when compared with sample A (Fig. 2a). This has indicated the reduction in the degree of binding of water on the surface of bigger crystallites, due to the less atoms/surface unit for the binding interaction with water molecules. The band shift from  $3476$  to  $3438\text{ cm}^{-1}$ , and from  $1636$  to  $1627\text{ cm}^{-1}$ , for the sample A compared to the sample B may be assumed to be attributable to more hydrogen bonding in the sample B due to the presence of more defect sites. This band can be assigned to the vibrations of water molecules/the formation of hydrogen bonds between and/or hydroxyl groups. In general, this shift of the absorption peaks toward the red shift in  $\text{Al}-\text{OH}$  suggests that the  $\text{Ni}-\text{OH}$  groups were changed and transformed to the  $\text{Al}-\text{O}-\text{Ni}$  bonds [21]. Fig. 2(a and b) shows the metal–oxygen stretching fre-

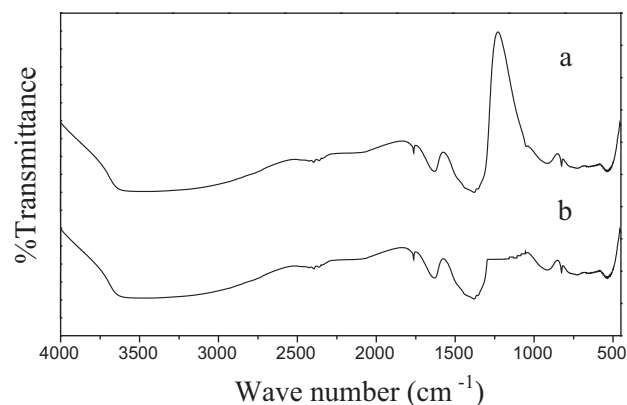


**Figure 2** FT-IR spectra of (a)  $\text{NiAl}_2\text{O}_4$ -sample A prepared by CCM (b)  $\text{NiAl}_2\text{O}_4$ -sample B prepared by MCM.

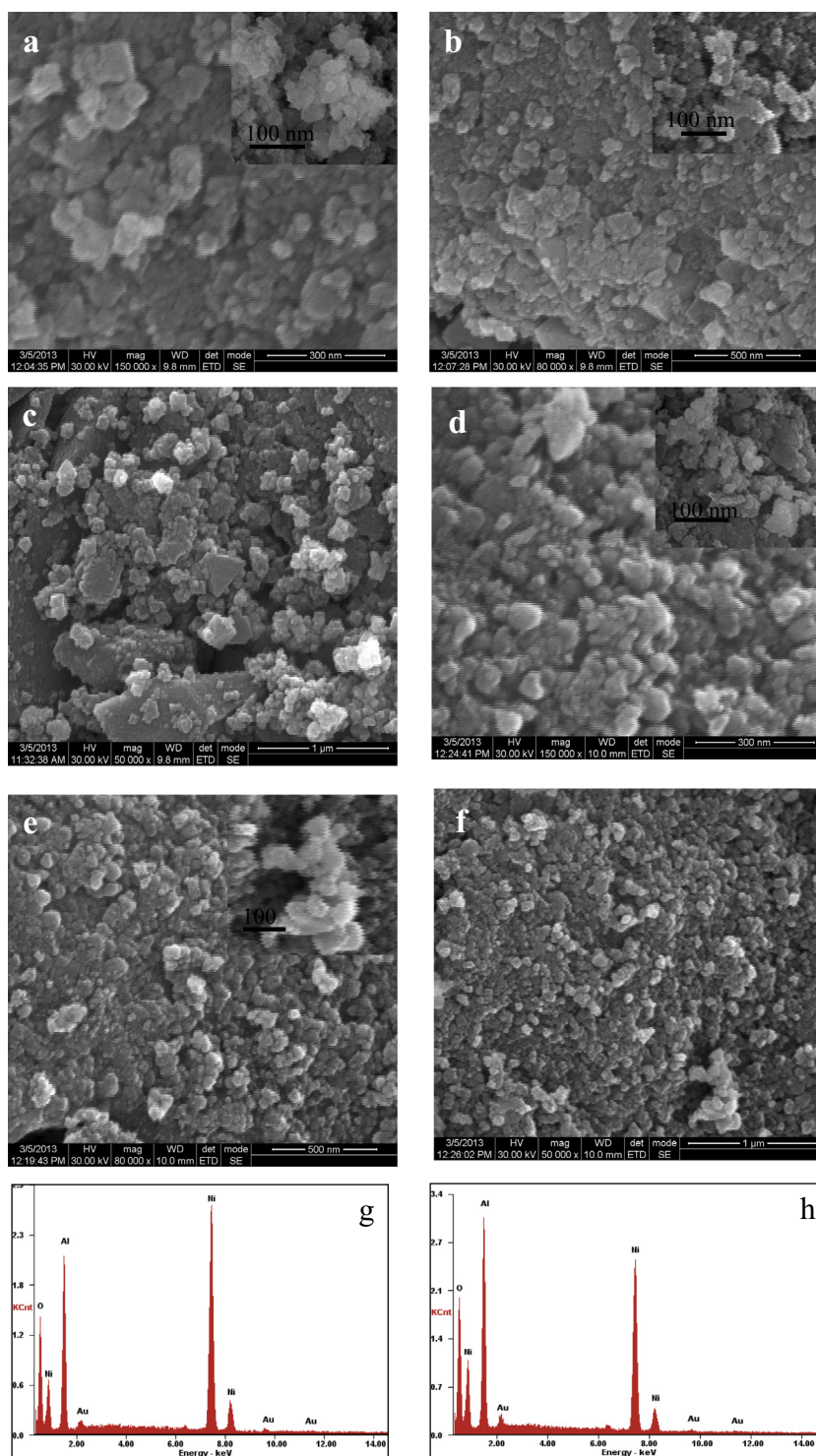


**Figure 3** HR-SEM images of  $\text{NiAl}_2\text{O}_4$ : (a-c) sample A prepared by CCM (d-f) sample B prepared by MCM., EDX spectrum of  $\text{NiAl}_2\text{O}_4$ : (g) sample A prepared by CCM (h) sample B prepared by MCM.

quencies in the range  $450\text{--}900\text{ cm}^{-1}$ , which are associated with the vibrations of M–O, Al–O, and M–O–Al bonds.  $\text{NiAl}_2\text{O}_4$  was formed as a mixture of the normal spinel ( $\text{Al}^{3+}$  ions in octahedral sites of  $\text{AlO}_6$  groups) and the inverse spinel ( $\text{Al}^{3+}$  ions in octahedral  $\text{AlO}_6$  and tetrahedral  $\text{AlO}_4$  sites). These spectra show the presence of three bands centered at 827–

811, 722–720, and of 525–523  $\text{cm}^{-1}$ , respectively. The Al–O and Ni–O stretching frequencies are found in the range 900–450 and 850–500  $\text{cm}^{-1}$ , respectively. The characteristic Al–O–Ni frequencies ( $450\text{--}850\text{ cm}^{-1}$ ) present in the molecule are also observed indicating the formation of single-phase  $\text{NiAl}_2\text{O}_4$  [23].

The absorption at  $2000\text{--}900\text{ cm}^{-1}$  corresponds to the deformation mode of Al–OH and Ni–OH, which are typical of this class of materials. In addition, the strong multiple bands in the region  $2000\text{--}900\text{ cm}^{-1}$  ( $1770\text{--}1753$ ,  $1630\text{--}1623$ ,  $1385\text{--}1376$  and  $925\text{--}909\text{ cm}^{-1}$ ) are essentially due to  $\text{OH}^-$  deformation modes of hydrogen-bonded –OH. The weak absorption band at  $2080\text{--}2073\text{ cm}^{-1}$  has been attributed to the existence of intercalated carbonate ions. The strong absorption band at  $2388\text{--}2371\text{ cm}^{-1}$  originates from the mode of  $\text{CO}_2^{3-}$  ion. The presence of this  $\text{CO}_2$  is either because of the presence of aerial  $\text{CO}_2$  or may be because of the presence of  $\text{CO}_2$  inside the grains of powders [5]. For instance, the three bands are shifted to  $827\text{--}811$ ,  $722\text{--}720$ , to either and  $525\text{--}523\text{ cm}^{-1}$ , respectively. With respect to samples A and B, all these absorption peaks shifting higher to lower wavenumbers is considered an indication of the combination to form nickel aluminate [16]. These bands correspond to  $\text{AlO}_6$  units, which built up the  $\text{NiAl}_2\text{O}_4$  spinel, thus indicating the formation of  $\text{NiAl}_2\text{O}_4$  spinels. For a nanosize grain, the atomic arrangements on the boundaries differed greatly from those of bulk crystals both in co-ordination number and bond lengths, which showed some extent of disorder [1,7,29]. No other impurity phase was detected by FT-IR spectra, and was in good agreement with the results obtained by XRD.

### 3.3. High resolution scanning electron microscopy (HR-SEM) studies

The surface morphology of the samples A and B was investigated by high resolution scanning electron microscopy. The HR-SEM images of  $\text{NiAl}_2\text{O}_4$  prepared by both CCM and MCM are shown in Fig. 3(a–c) and (d–f), respectively. Therefore, we could infer that the  $\text{NiAl}_2\text{O}_4$  nanoparticles were formed in both CCM and MCM.

In CCM, the reaction was completed only after 3 h, whereas in MCM, the reaction was completed within few minutes. Within the limited time, nucleation and growth had to be finished. Hence, the particles with smaller and narrow distribution were obtained by MCM. However, in CCM, the time might be sufficient to form the separate phases, which has led to the bigger particle size of 19.9 nm with wider distribution, but in the microwave method, the size of the particle is only 16.4 nm. The observed slight difference in particle size value as estimated from the two different techniques (XRD and HR-SEM) may be due to some structural disorder and strain in the lattice resulting from different ionic radii and/or clustering of the nanomaterials.

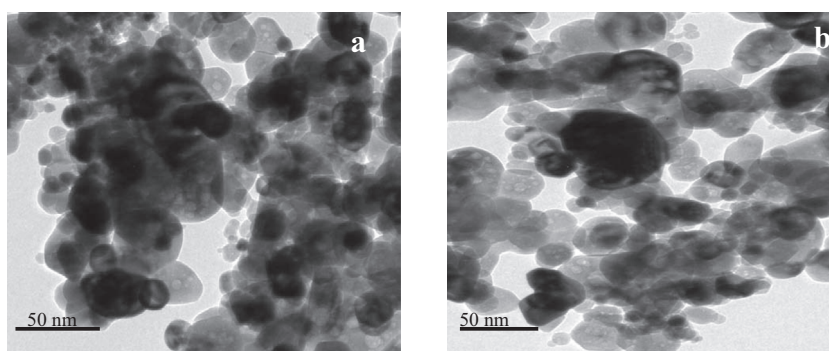


**Figure 4** HR-TEM images of  $\text{NiAl}_2\text{O}_4$ : (a) sample A prepared by CCM (b) sample B prepared by MCM.

The presence of  $\text{NiAl}_2\text{O}_4$  was also confirmed by means of energy dispersive X-ray analysis (EDX) as shown in Fig. 3(g and h). It exhibited Ni, Al, and O peaks and indicated the presence of  $\text{NiAl}_2\text{O}_4$  phase without any other impurity. It is in good agreement with the XRD analysis. The peaks at 2.1–2.2 keV in the EDX spectra were due to the gold coated on the samples before recording HR-SEM.

### 3.4. High resolution transmission electron microscopy (HR-TEM) studies

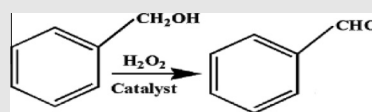
In order to further confirm the morphology, HR-TEM studies are carried out. The presence of  $\text{NiAl}_2\text{O}_4$  nanoparticles of bigger size for the sample A is shown in Fig. 4a. Fig. 4b shows the presence of  $\text{NiAl}_2\text{O}_4$  nanoparticles of smaller size obtained from sample B prepared by MCM. Moreover, the particles prepared under microwave irradiation were of narrower distribution than those prepared by the conventional method. The obtained particles are nearly spherical in shape with a uniform size distribution for sample B.

### 3.5. $\text{N}_2$ adsorption/desorption isotherms

The nitrogen adsorption/desorption isotherm values at 77 K of the samples A and B are given in Table 1. Surface area parameters of the samples varied according to the preparation method. The nickel aluminate (sample A) prepared by CCM route possessed a surface area of  $75.73\text{ m}^2/\text{g}$ , whereas for sample B prepared by MCM, the BET surface area is increased considerably to  $107.34\text{ m}^2/\text{g}$ . The pore volumes of the samples A and B are  $0.9597\text{ cm}^3/\text{g}$  and  $0.0797\text{ cm}^3/\text{g}$ , respectively. Similarly, the average pore radius of the sample A is  $26.97\text{ \AA}$ , but for the sample B, it is only  $14.54\text{ \AA}$ . The average pore radius of

**Table 1** BET surface area, average pore radius and pore volume of  $\text{NiAl}_2\text{O}_4$  samples prepared by using plant extract.

Sample	BET surface area ( $\text{m}^2/\text{g}$ )	Average pore radius ( $\text{\AA}$ )	Total pore volume ( $\text{cm}^3/\text{g}$ )
Sample A	75.73	26.97	0.9597
Sample B	107.34	14.54	0.0797



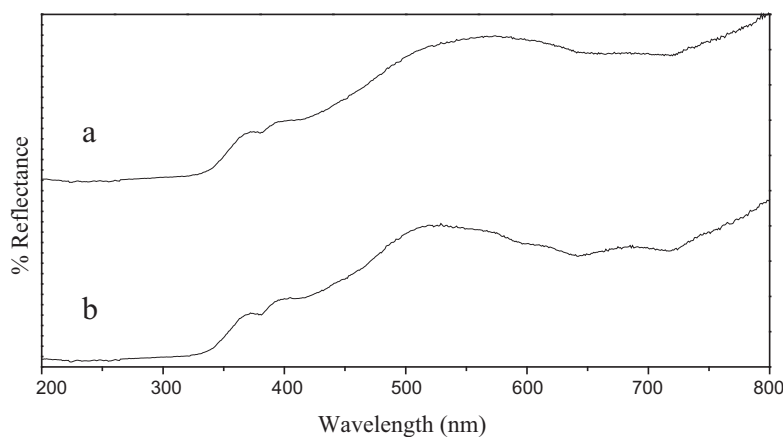


**Figure 5** Diffuse reflectance spectra of (a)  $\text{NiAl}_2\text{O}_4$ -sample A prepared by CCM (b)  $\text{NiAl}_2\text{O}_4$ -sample B prepared by MCM.

the samples is due to the formation of intergranular particles within the combination of metal oxides. The decrease in the average pore radius for sample B can be attributed to the reduction in grain size, which is later confirmed by HR-SEM and/TEM studies. This shows that MCM is a more powerful technique, and can achieve the same results with a shorter time when compared to the CCM.

### 3.6. Diffuse reflectance spectroscopy (DRS) studies

The  $\text{Ni}^{2+}$  species in nickel aluminate spinel with electronic configuration of  $3d^8$ , can exist in tetrahedral and octahedral coordination sites. The occupancy of octahedral and tetrahedral sites by  $\text{Ni}^{2+}$  depends on the temperature and in either case; there are five allowed transitions and some other spin forbidden transitions [9]. Fig. 5(a and b) shows the UV-Vis-DRS profiles of the sample prepared in the present study. The bands at 360–380 nm, 390–410 nm and 700–722 nm were assigned to the octahedrally coordinated  $\text{Ni}^{2+}$  species in NiO lattice, while those at 500–550 nm and in the range of 600–645 nm were related to the tetrahedrally coordinated  $\text{Ni}^{2+}$  species in the nickel aluminate lattice [19]. Nevertheless, the UV region could provide useful information about the presence of the octahedral Ni (II) cations. The high energy region (200–500 nm) contains usually the charge transfer bands, but the clear shoulder identified at ca. 360–380 nm is characteristic to the octahedral Ni (II) cations in NiO. Nickel aluminate (A and B) catalyst exhibits stronger intense UV-DRS band at 500–645 nm thus confirming the presence of single phase nickel aluminate spinel, as confirmed by XRD. These results are in agreement with the estimated octahedral/tetrahedral occupancy degree for the two nickel aluminate oxides. These bands are attributed to  $\text{Ni}^{2+}$  in octahedral sites and  $\text{Al}^{3+}$  in tetrahedral sites, respectively. The Al 3p ions occupy both the tetrahedral A- and the octahedral B-sites in equal amounts. The Ni 2p ions occupy only the B-sites and this causes the tetragonal distortion, due to the Jahn–Teller effect [31,13,22].

### 3.7. Catalytic oxidation of benzyl alcohol using sample A and B

The catalytic oxidation of benzyl alcohol was studied using nickel aluminate nanoparticles to investigate its catalytic performance. 0.5 g of samples A or B along with the  $\text{H}_2\text{O}_2$  as ox-

idant (5 mmol) in acetonitrile medium was taken in a batch reactor, and the contents were heated at 80 °C for 8 h. When the oxidized product was analyzed using gas chromatography (GC), it showed the conversion and selectivity of the benzaldehyde. It was noticed that the nano nickel aluminate possessed a higher yield with good selectivity for benzaldehyde. The method of preparation proposed in the present study was very simple and economic. Hence, the addition of *O. dilenii haw* plant extract during the preparation stage enhanced the catalytic properties of nickel aluminate. It was found that the surface area of the samples varied according to the preparation either by CCM and MCM. From Table 2, it is formed that the nano nickel aluminate sample A possessed a surface area of 75.73  $\text{m}^2/\text{g}$ , whereas for sample B, the BET surface area was increased considerably to 107.34  $\text{m}^2/\text{g}$ . The results indicated that the conversion of benzyl alcohol increased to 89.38% and selectivity of 99.99% was achieved, when the sample B was used. Using Sample A low conversion of 68.51% was achieved with the selectivity of 97.22% [20].

### 3.8. Effect of solvent

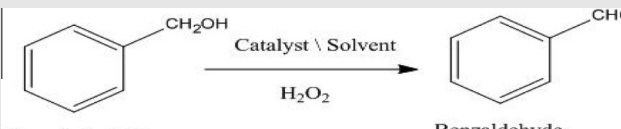
From the results, it was found that the nano nickel aluminate prepared by CCM (sample A) and MCM (sample B) was found to be highly active toward the selective oxidation of benzyl alcohol to benzaldehyde. The sample B was found to be the most active and selective one for the benzyl alcohol oxidation reaction and higher than sample A, as expected from its surface area (107.34  $\text{m}^2/\text{g}$ ) and lower crystallite size (16.4 nm). The effect of solvent on the conversion of benzyl alcohol and benzaldehyde selectivity is given in Table 3. In the presence of acetonitrile, a high conversion with (90%) better selectivity

**Table 2** Surface area properties of nickel aluminate samples A and B and their activity in benzyl alcohol oxidation.

Catalyst	BET surface area ( $\text{m}^2/\text{g}$ )	Conversion (%)	Selectivity (%)
Sample A	75.73	68.51	97.22
Sample B	107.54	89.38	99.99

*Reaction conditions:* Catalyst (samples A and B)  $\text{NiAl}_2\text{O}_4$ , 0.5 g; benzyl alcohol, 5 mmol; acetonitrile, 5 mmol;  $\text{H}_2\text{O}_2$ , 5 mmol; temperature, 80 °C, time, 8 h.

**Table 3** Effect of solvent on the conversion and selectivity percentage for the oxidation of benzyl alcohol by sample A prepared by CCM and sample B prepared by MCM.



Sample	Solvent	Conversion (%)	Selectivity (%)
Sample A	Acetonitrile	70.5	97.2
	DMSO	76.3	86.1
	DMF	74.2	85.2
Sample B	Acetonitrile	90.0	99.9
	DMSO	82.9	91.2
	DMF	77.7	88.7

*Reaction conditions:* Catalyst (sample A and B)  $\text{NiAl}_2\text{O}_4$ , 0.5 g; benzyl alcohol, 5 mmol; solvent, 5 mmol;  $\text{H}_2\text{O}_2$ , 5 mmol; temperature, 80 °C, time, 8 h.

(99%) is observed, than in the presence of other solvents like DMF and DMSO. It is mostly due to the competitive adsorption between the solvent and benzyl alcohol on the catalyst and thereby adsorbed solvent molecules occupying a part of the active sites of the catalyst. Even though, acetonitrile is polar and having a very high dielectric constant, it may readily dissolve  $\text{H}_2\text{O}_2$  along with the benzyl alcohol, and consequently will direct the reactants in such a way that it can properly be adsorbed on the catalyst surface, thereby increasing the efficiency of the conversion. In addition, the relatively high solubility of  $\text{O}_2$  in acetonitrile has accelerated the oxidation reaction [26,25]. The high conversion might be because of acetonitrile being a good solvent and also a stoichiometric oxidant, which could promote a better selectivity toward the benzaldehyde [34].

Also, acetonitrile can activate the peroxide by forming a perhydroxyl anion ( $\text{OOH}^-$ ) that nucleophilically attacks the nitrile to generate a peroxy-carboximidic acid intermediate, which is a good oxygen transfer agent. Both the organic substrates as well as the oxidant  $\text{H}_2\text{O}_2$  dissolve in acetonitrile forming a uniform solution [28]. Therefore, acetonitrile was

chosen as the best solvent for the selective oxidation of benzyl alcohol.

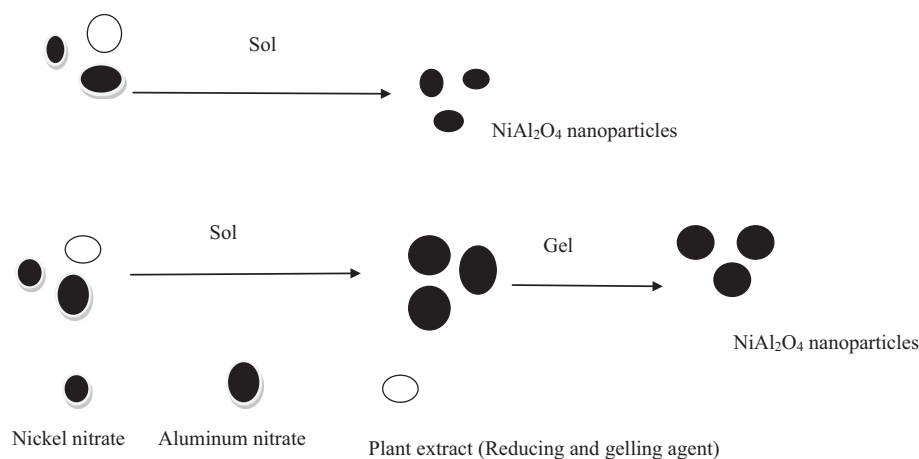
### 3.9. Comparison between CCM and MCM

Microwave and conventional heating systems are used successfully for synthesizing nickel aluminate nanoparticles via a solution combustion synthesis, using metal nitrates and plant extract as raw materials. For both the heating methods, the resultant powder was fine, brittle and nanocrystalline, in which  $\text{NiAl}_2\text{O}_4$  nanoparticles were homogeneously dispersed. The results proved that the microwave heating system is a fast and easy synthesis method, in which there is no need for preparing the gel; and the solution can directly interact with the microwave signals and results in a well-developed combustion reaction. While, in the conventional heating, the sol should be changed to gel and then converted to the product, due to high temperature heating in a furnace. Furthermore, the final powder produced in microwave heating system has finer crystallites with narrower size distribution in contrast with the sample prepared in the furnace with the same starting raw materials (Scheme 1). Nevertheless the specific surface area of the sample prepared in furnace, using gel as starting precursor is higher in comparison with the sample prepared in microwave, in which the sol was used as the starting precursor. This is due to the fact that the microwave heating is volumetric and uniform when compared to the conventional furnace heating, which is non-uniform and radiative. Thus, it could be postulated that the microwave field has an overall influence on the reaction rate nanoparticle size and shape control.

From Table 3, it is found that in all the three solvent mediums, sample B prepared by MCM showed higher conversion with better selectivity than the one prepared by CCM (sample A). Thus, microwave combustion synthesized sample exhibits better performance, because of the above stated reasons [27].

## 4. Conclusions

In the present work, nickel aluminate spinel was prepared by CCM and MCM using *O. dilenii haw* as the plant extract solution. The formation of nickel aluminate phase was confirmed by XRD and FT-IR. The nanoparticles prepared by the micro-



**Scheme 1** Proposed schematic model for the synthesis process of  $\text{NiAl}_2\text{O}_4$  nanoparticles prepared by the conventional combustion method (CCM) and the microwave combustion method (MCM).

wave method were smaller in the size and more narrowly distributed, greater catalytic activity of benzyl alcohol to benzaldehyde was obtained for the sample prepared MCM, than the one prepared by CCM. Compared with the CCM, the microwave-assisted method is more time-saving. Hence, in the present study, we have reported the simple and rapid microwave synthetic method for the synthesis of nickel aluminate nanoparticles in the turnable optical and better catalytic properties.

## References

- [1] S. Angappan, L.J. Bechemans, C.O. Augustin, Sintering behaviour of  $MgAl_2O_4$ -a prospective anode material, *Mater. Lett.* 58 (2004) 2283–2289.
- [2] D. Bhattacharya, G. Rajinder, Nanotechnology and potential of microorganisms, *Crit. Rev Biotechnol.* 25 (2005) 199–204.
- [3] A. Becheri, M. Durr, P. Lo Nostro, P. Baglioni, Synthesis and characterization of zinc oxide nanoparticles: application to textiles as UV-absorbers, *J. Nanopart. Res.* 10 (2008) 679–689.
- [4] R. Boubekri, Z. Beji, K. Elkabous, F. Herbst, G. Viau, S. Ammar, F. Fievet, H.J. von Bardeleben, A. Mauger, Annealing effects on  $Zn(Co)O$ : From para-to ferromagnetic behavior, *Chem. Mater.* 21 (2009) 843–855.
- [5] Z. Chen, E. Shi, W. Li, Y. Zheng, N. Wu, W. Zhong, Particle size comparison of hydrothermally synthesized cobalt and zinc aluminate spinels, *J. Am. Ceram. Soc.* 85 (2002) 2949–2955.
- [6] S. Chokkaram, R. Srinivasan, D.R. Milburn, B.H. Davis, Conversion of 2-octanol over nickel–alumina, cobalt–alumina, and alumina catalysts, *J. Mol. Catal. A: Chem.* 121 (1997) 157–169.
- [7] M. Chroma, J. Pinkas, I. Pakutinskiene, A. Beganskiene, A. Kareiva, Processing and characterization of sol–gel fabricated mixed metal aluminates, *Ceram. Int.* 31 (2005) 1123–1130.
- [8] F. Deganello, G. Marci, G. Deganello, Citrate–nitrate auto-combustion synthesis of perovskite-type nanopowders: a systematic approach, *J. Eur. Ceram. Soc.* 29 (2009) 439–450.
- [9] S.O. Dumont, Spectrophotometrical investigations on the structural characteristics of oxide lattices containing transition metals, *Bull. Soc. Chim. Fr.* 105 (1965) 1099–1105.
- [10] T.T. Emons, J.Q. Li, L.F. Nazarm, Synthesis and characterization of mesoporous indium tin oxide possessing an electronically conductive framework, *J. Am. Chem. Soc.* 124 (2003) 8516–8517.
- [11] E.M. Galati, S. Pergolizzi, N. Miceli, M.T. Monforte, M.M. Tripodo, Study on the increment of the production of gastric mucus in rats treated with *Opuntia ficus indica* (L.) Mill, *Cladodes. J. Ethnopharmacol.* 83 (2002) 229–233.
- [12] V.V. Gulians, M.A. Carreon, Y.S. Lin, Ordered mesoporous and macroporous inorganic films and membranes, *J. Membr. Sci.* 235 (2004) 53–72.
- [13] D. Gingsu, I. Mindru, L. Patron, C.B. Cizmas, Tetragonal copper ferrite obtained by self-propagating combustion, *J. Alloys Compd.* 460 (2008) 627–631.
- [14] X. Hu, J.C. Yu, J. Gong, Fast production of self-assembled hierarchical  $\alpha$ - $Fe_2O_3$  nanoarchitectures, *J. Phys. Chem. C* 111 (2007) 1180–1185.
- [15] F. Hassan, A. El-Razek, A.A. Hassan, Nutritional value and hypoglycemic effect of *Prickly Cactus Pear (Opuntia Ficus-Indica)* fruit juice in alloxan-induced diabetic rats, *Aust. J. Basic. Appl. Sci.* 5 (2012) 356–377.
- [16] M. Janga, J.K. Park, E.W. Shin, Lanthanum functionalized highly ordered mesoporous media: implications of arsenate removal, *Microporous Mesoporous Mater.* 75 (2004) 159–168.
- [17] P. Jeevanandam, Yu. Koltypin, A. Gedanken, Preparation of nanosized nickel aluminate spinel by a sonochemical method, *Mater. Sci. Eng. B* 90 (2002) 125–132.
- [18] A.G. Khaledi, S. Afshar, H.S. Jahromi, Improving  $ZnAl_2O_4$  structure by using chelating agents, *Mater. Chem. Phys.* 135 (2012) 855–862.
- [19] P. Kim, Y. Kim, H. Kim, I.K. Song, J. Yi, Preparation of nickel mesoporous materials and their application to the hydrodechlorination of chlorinated organic compounds, *Appl. Catal. A-Gen.* 272 (2004) 157–166.
- [20] R.T. Kumar, P. Suresh, N.C.S. Selvam, L.J. Kennedy, J.J. Vijaya, Comparative study of nano copper aluminate spinel prepared by sol–gel and modified sol–gel techniques: structural, electrical, optical and catalytic studies, *J. Alloys Compd.* 522 (2012) 39–45.
- [21] S.C. Laha, P. Mukherjee, S.R. Sainkar, R. Kumar, Cerium containing MCM-41-type mesoporous materials and their acidic and redox catalytic properties, *J. Catal.* 207 (2002) 213–223.
- [22] P. Laokul, V. Amornkitbamrung, S. Seraphin, S. Maensiri, Characterization and magnetic properties of nanocrystalline  $CuFe_2O_4$ ,  $NiFe_2O_4$ ,  $ZnFe_2O_4$  powders prepared by the aloe vera extract solution, *Curr. Appl Phys.* 11 (2011) 101–108.
- [23] F. Meyer, R. Hempelmann, S. Mathurband, M. Veith, Microemulsion mediated sol–gel synthesis of nano-scaled  $MAI_2O_4$  ( $M=Co, Ni, Cu$ ) spinels from single-source heterobimetallic alkoxide precursors, *J. Mater. Chem.* 9 (1999) 1755–1763.
- [24] R.D. Monte, J. Kaspar, Nanostructured  $CeO_2$ – $ZrO_2$  mixed oxides, *J. Mater. Chem.* 15 (2005) 633–648.
- [25] C. Mondelli, D. Ferri, J.D. Grunwaldt, F. Krumeich, S. Mangold, R. Psaro, A. Baiker, Combined liquid-phase ATR-IR and XAS study of the Bi-promotion in the aerobic oxidation of benzyl alcohol over  $Pd/Al_2O_3$ , *J. Catal.* 252 (2007) 77–87.
- [26] M.S. Niasari, F. Davar, Synthesis, characterization and catalytic activity of copper (II) complexes of 14-membered macrocyclic ligand; 3,10-dialkyl-dibenzo-1,3,5,8,10,12-hexaazacyclotetradecane/zeolite encapsulated nanocomposite materials, *Inorg. Chem. Commun.* 9 (2006) 304–309.
- [27] L. Perreux, A. Loupy, A tentative rationalization of microwave effects in organic synthesis according to the reaction medium and mechanistic considerations, *Tetrahedron* 57 (2001) 9199–9223.
- [28] U.R. Pillai, E. Sahle-Demessie, Selective oxidation of alcohols over vanadium phosphorus oxide catalyst using hydrogen peroxide, *Appl. Catal. A: Gen.* 276 (2004) 139–144.
- [29] Z. Peng, X. Fu, H. Ge, Z. Fu, C. Wang, L. Qi, H. Miao, Effect of  $Pr^{3+}$  doping on magnetic and dielectric properties of Ni–Zn ferrites by “one-step syntheses”, *J. Magn. Mater.* 323 (2011) 2513–2518.
- [30] J.C. Rodriguez, A.J. Marchi, A. Borgna, A. Monzon, Effect of Zn content on catalytic activity and physicochemical properties of Ni-based catalysts for selective hydrogenation of acetylene, *J. Catal.* 171 (1997) 268–278.
- [31] B. Scheffer, J.J. Heijeinga, J.A. Moulijn, An electron spectroscopy and X-ray diffraction study of nickel oxide/alumina and nickel-oxide-tungsten trioxide/alumina catalysts, *J. Phys. Chem.* 91 (1987) 4752–4759.
- [32] P. Salagre, J.L.G. Fierro, F. Medina, J.E. Sueiras, Characterization of nickel species on several  $\gamma$ -alumina supported nickel samples, *J. Mol. Catal. A: Chem.* 106 (1996) 125–134.
- [33] E. Satoh, T. Ishii, Y. Shimizu, S. Sawamura, M. Nishimura, Black tea extract, the arubigin fraction, counteracts the effect of tetanus toxin in mice, *Proc. Soc. Exp. Biol. Med.* 226 (2001) 577–580.
- [34] B.A. Steinhoff, S.S. Stahl, Mechanism of  $Pd(OAc)_2$ /DMSO-catalyzed aerobic alcohol oxidation: mass-transfer-limitation effects and catalyst decomposition pathways, *J. Am. Chem. Soc.* 128 (2006) 4348–4355.



- [35] N.J. Van der Laag, M.D. Snel, P.C.M.M. Magusin, G. de With, Structural, elastic, thermo physical and dielectric properties of zinc aluminate, *J. Eur. Ceram. Soc.* 24 (2004) 2417–2424.
- [36] J.J. Vijaya, L.J. Kennedy, G. Sekaran, K.S. Nagaraja, Sol–gel derived (Sr, Ni)  $Al_2O_4$  composites for benzene and toluene sensors, *Mater. Lett.* 61 (2007) 5213–5216.
- [37] J.J. Vijaya, L.J. Kennedy, G. Sekaran, K.S. Nagaraja, Synthesis, characterization and humidity sensing properties of Cu–Sr–Al mixed metal oxide composites, *Mater. Res. Bull.* 43 (2008) 473–482.
- [38] R. Veerasamy, T.Z. Xin, S. Gunasagan, T.F.W. Xiang, E.F.C. Yang, N. Jeyakumar, S.A. Dhanaraj, Biosynthesis of silver nanoparticles using mangosteen leaf extract and evaluation of their antimicrobial activities, *J. Saudi Chem. Soc.* 15 (2011) 113–120.
- [39] F. Zhou, X. Zhao, C. Yuan, L. Li, Vanadium pentoxide nanowires: hydrothermal synthesis, formation mechanism, and phase control parameters, *Cryst. Growth Des.* 8 (2008) 723–727.